Ann Nucl Med (2014) 28:961–969
DOI 10.1007/s12149-014-0892-z

ORIGINAL ARTICLE

Ultrahigh-resolution Cerenkov-light imaging system for positron radionuclides: potential applications and limitations

Seiichi Yamamoto · Tadashi Watabe · Hayato Ikeda · Yasukazu Kanai · Hiroshi Watabe · Yoshimune Ogata · Katsuhiko Kato · Jun Hatazawa

Received: 2 June 2014 / Accepted: 29 July 2014 / Published online: 8 August 2014

Abstract
Objective Cerenkov-light imaging provides inherently high resolution because the light is emitted near the positron radionuclide. However, the magnitude for the high spatial resolution of Cerenkov-light imaging is unclear. Its potential molecular imaging applications also remain unclear. We developed an ultrahigh-resolution Cerenkov-light imaging system, measured its spatial resolution, and explored its applications to molecular imaging research.
Methods Our Cerenkov-light imaging system consists of a high-sensitivity charged-coupled device camera (Hamamatsu Photonics ORCA2-ER) and a bright lens (Xenon 0.95/25). An extension ring was inserted between them to magnify the subject. A ~100-μm-diameter ^{22}Na point source was made and imaged by the system. For applications of Cerenkov-light imaging, we conducted ^{18}F-FDG administered in vivo, ex vivo whole brain, and sliced brain imaging of rats.
Results We obtained spatial resolution of ~220 μm for a ^{22}Na point source with our developed imaging system. The ^{18}F-FDG rat head images showed high light intensity in the eyes for the Cerenkov-light images, although there was no accumulation in these parts in the PET images. The sliced rat brain showed much higher spatial resolution for the Cerenkov-light images compared with $CdWO_4$ scintillator-based autoradiography, although some contrast decrease was observed for them.
Conclusion Even though the Cerenkov-light images showed ultrahigh resolution of ~220 μm, their distribution and contrast were sometimes different from the actual positron accumulation in the subjects. Care must be taken when evaluating positron distribution from Cerenkov-light images. However, the ultrahigh resolution of Cerenkov-light imaging will be useful for transparent subjects including phantom studies.

Keywords Cerenkov-light imaging · Ultrahigh resolution · CCD camera · Positron · Molecular imaging

Introduction

Cerenkov-light imaging [1, 2] is a relatively new molecular imaging technology that images the distribution of radionuclides that emit positrons or electrons using a high-sensitivity optical camera. The positrons or electrons emit a small amount of light called Cerenkov light when their energies exceed a threshold level that is determined by the refractive index of the materials [3]. In Cerenkov-light imaging of molecular imaging, such light distribution is imaged by a high-sensitivity cooled charge-coupled device (CCD) camera. Some small animal images using Cerenkov-light imaging have already been reported [1, 2, 4–12].

Figure 1 shows a schematic drawing of the relation of the positron range and the emission of Cerenkov light. The range of the beta or the positron is determined by the distance from the positron radionuclide to the point of annihilation (when the beta or positron energy becomes zero). The Cerenkov light is emitted when the positron's

S. Yamamoto (✉) · Y. Ogata · K. Kato
Department of Radiological and Medical Laboratory Sciences, Nagoya University Graduate School of Medicine, 1-1-20 Daiko-Minami, Higashi-ku, Nagoya 461-8673, Japan
e-mail: s-yama@met.nagoya-u.ac.jp

T. Watabe · H. Ikeda · Y. Kanai · J. Hatazawa
Osaka University Graduate School of Medicine, Suita, Japan

H. Watabe
Tohoku University, Sendai, Japan

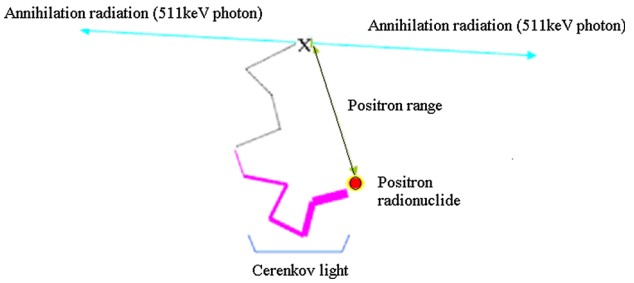

Fig. 1 Schematic of relation between Cerenkov-light emission and range for positron emitting radionuclide

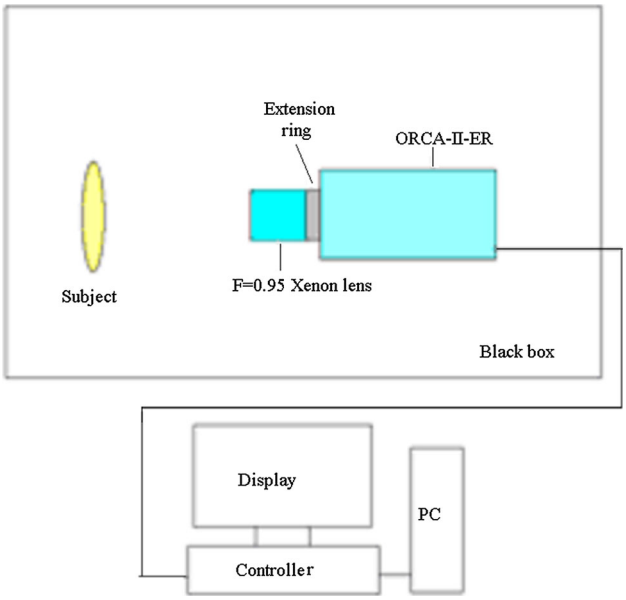

Fig. 2 Schematic drawing of the developed Cerenkov-light imaging system

energy exceeds the threshold level ($\sim$260 keV for biologic tissue [13, 14]). Since Cerenkov light's intensity is higher for greater positron energy, the gravity of Cerenkov-light emission approaches the radionuclide. Higher spatial resolution can be obtained with Cerenkov-light imaging than positron emission tomography (PET). For ^{18}F, the line spread function was reported to be $\sim$350-μm FWHM with a width of 200-μm ^{18}F positron line source [4].

Although high spatial resolution is expected with Cerenkov-light imaging, the precise measurement of spatial resolution has not been reported yet, probably because of the difficulty of the preparation of the small diameter positron source. Its potential applications to molecular imaging are also unclear. To clarify these points, we developed an ultrahigh-resolution Cerenkov-light imaging system, measured its spatial resolution, and explored its applications to molecular imaging research. We conducted Cerenkov-light imaging for phantoms as well as ^{18}F-FDG administered in vivo and ex vivo rat studies for this purposes.

Materials and methods

Cerenkov-light imaging system

For imaging Cerenkov light from positron radionuclide distribution, we used a high-sensitivity cooled CCD camera (ORCA2-ER, Hamamatsu Photonics, Japan) operated in minus 60 °C. We show a schematic drawing of a developed Cerenkov-light imaging system in Fig. 2. A bright lens (Xenon 0.95/25) was mounted on the camera and placed in a black box. Signals from the CCD camera were fed to the controller and a personal computer (PC). An extension lens was inserted between the camera and lens to take magnified images. We show a photo of the CCD camera and the black box that contained the high-sensitivity CCD camera in Fig. 3a, b. The parameters of the CCD camera for Cerenkov-light imaging were under the following imaging conditions—gain: 2, light mode: 0, scan speed: 1, and 2 × 2 binning of the pixels.

One technical problem in Cerenkov-light imaging is the noise spots from the direct detection of gamma photons by the CCD sensor (direct noise). Normally, cosmic rays and environmental gamma photons are the main sources of direct noises, but the gamma photons from the positron radionuclide injected into the subject are a much bigger noise source. Direct noises have much higher intensity than Cerenkov-light images and create serious noises on them. We reduced the noise using noise removal outlier processing of ImageJ software on the Cerenkov-light images. The processing replaces a pixel by the median of the pixels in the surrounding if it deviates from the median by more than a certain value (the threshold) [15, 16]. It is useful for correcting hot pixels or dead pixels of a CCD camera. Because it had high intensity and a spot shape, most were eliminated by the software.

Performance evaluation of Cerenkov-light imaging system

1. *Spatial resolution* One possible advantage of Cerenkov-light imaging is higher spatial resolution. Thus, we first imaged a small point source of ^{22}Na using our Cerenkov-light imaging system to evaluate the spatial resolution. We used ^{22}Na source because of the long half-life and similar maximum positron energy as ^{18}F (^{22}Na: 0.55 MeV, ^{18}F: 0.64 MeV). We made a 100-μm-diameter ^{22}Na point source using a 100-μm-diameter ion exchanging resin to

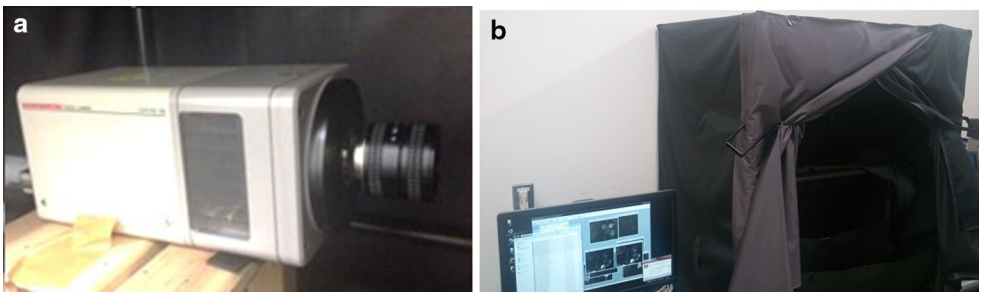

Fig. 3 High-sensitivity CCD camera for Cerenkov-light imaging (**a**) and *black box* used for measurements (**b**)

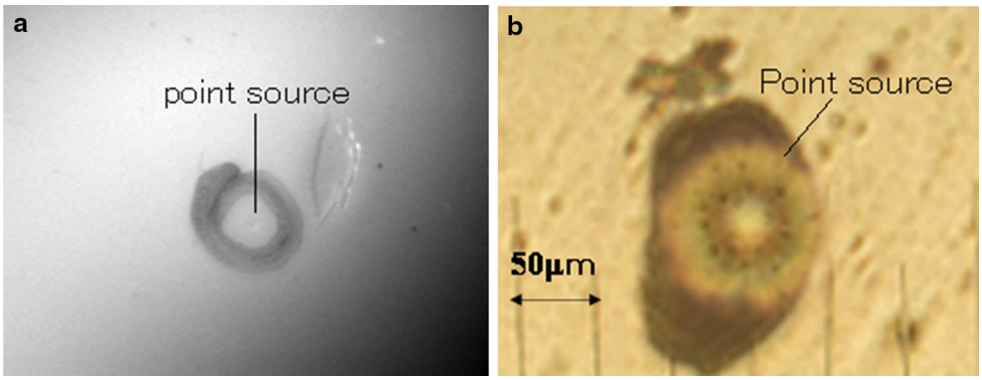

Fig. 4 Optical photo (**a**) and microscopic image (**b**) of a 100-µm point source

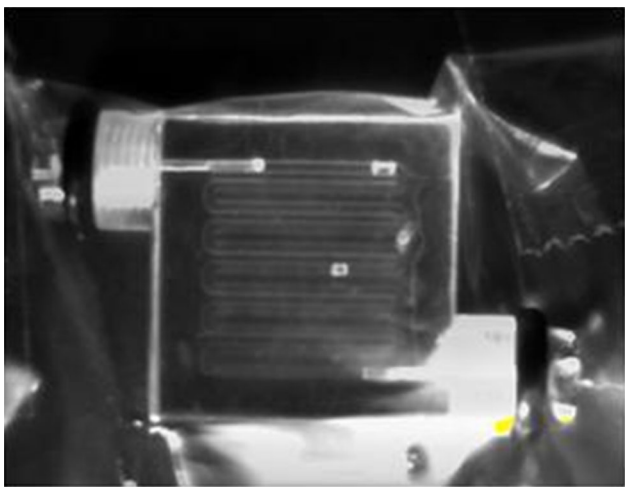

Fig. 5 Optical photo of the slit phantom

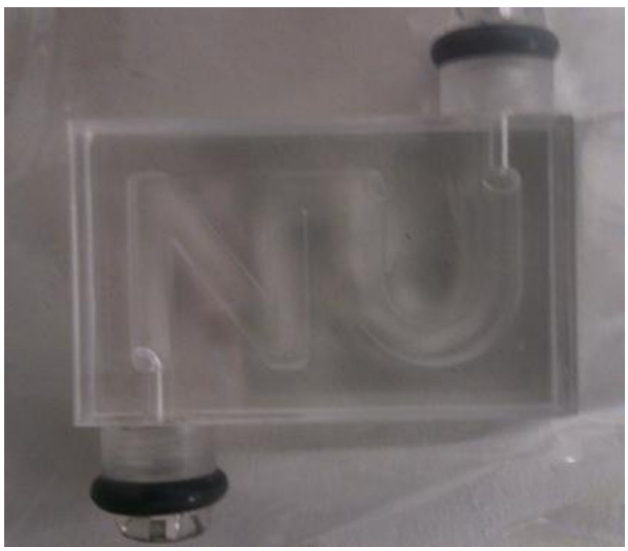

Fig. 6 Optical photo of the NU phantom

accumulate the ^{22}Na solution. After the accumulation of ^{22}Na, the point source's diameter was measured using an optical microscope (Olympus, IMT-2, Japan). We show an optical photo and a microscopic image of the point source in Fig. 4a, b.

The point source, which has 400-kBq activity, was placed in a 0.2-mm-thick sheet and sandwiched between 2-mm-thick acrylic plates. It was set ~10 mm from the lens surface of the CCD camera to measure the Cerenkov light. We imaged the point source for 10 s and set the profile on the image to evaluate the spatial resolution.

We also evaluated the spatial resolution by a slit phantom that contained ^{22}Na (Fig. 5). This slit phantom imaging is mainly for the demonstration of the high spatial resolution of Cerenkov-light imaging. The phantom's slits were 500 μm wide, and the separation was also 500 μm. The phantom contained 27 kBq of ^{22}Na solution.

2. *Imaging of character source phantom* Next, we measured the Cerenkov-light images of a distributed character phantom, which has the characters NU in which the ^{22}Na solution was contained. The purpose of this "NU" phantom imaging is not for evaluating the spatial resolution, but for the evaluation of image quality of the Cerenkov-light images including the signal to noise (S/N) of the images. An optical photo of the NU phantom, which contained 72 kBq of the ^{22}Na solution of the phantom's characters, is shown in Fig. 6. NU stands for Nagoya University. The dimension of the "NU" phantom is 25 mm × 15 mm and made of acrylic resin. We measured the Cerenkov-light images for 30–120 min to compare the image quality.

3. *Imaging of small animals* We measured the Cerenkov-light images of rats that were administered ^{18}F-FDG for in vivo and ex vivo studies. These studies were performed under the guidelines of the Laboratory Investigation Committee of the Osaka University Graduate School of Medicine. For in vivo rat studies, we conducted ^{18}F-FDG imaging on two nude rats with skin tumors. We also conducted head imaging on two normal rats without tumors. In the first study on nude rats with skin tumors, 40 MBq of ^{18}F-FDG was injected and Cerenkov-light imaging was conducted for 20 min, from 2 h after the injection. The imaging was done from the side of the rat. The second study on normal rats without skin tumors was conducted for 30 min, 1 h after the injection of 100 MBq ^{18}F-FDG. Imaging was conducted of the head and body parts from the rat's upper side.

In the first study on a normal rat without a tumor, we injected 150 MBq of ^{18}F-FDG and conducted Cerenkov-light imaging for 20 min, 2 h after the injection. Imaging was done from the upper side of the rat. In the second study on a normal rat without a tumor, imaging was conducted 80 min after the injection of 110 MBq of ^{18}F-FDG and measured for 30 min. Imaging was done for the head and body parts from the rat's upper side. For comparison, small animal PET imaging was conducted for the rat using Siemens Invion [17] for 10 min.

For all measurements except the last study, optical photo images were fused with Cerenkov-light images using ImageJ software. In the last study, we made fused images with Cerenkov light and a maximum intensity projection image of PET using ImageJ software.

For the ex vivo rat studies, we conducted two brain studies on rats that were administered ^{18}F-FDG: whole and sliced brain studies. Ex vivo whole brain Cerenkov-light imaging was conducted on a normal rat that was administered 150 MBq of ^{18}F-FDG, 2 h after the injection, and measured for 20 min. The ex vivo Cerenkov imaging of the sliced brain was conducted for 120 min, 2 h after the injection of 150 MBq ^{18}F-FDG, in 2-mm-thick slices. For comparison, imaging with a $CdWO_5$ (CWO) scintillator (0.1-mm thick) was conducted 5 h after the injection for 5 min. We set profiles for both images using ImageJ software to compare the sharpness of the edges.

Results

Performance evaluation of Cerenkov-light imaging system

1. *Spatial resolution* We show the image and the profile of a ^{22}Na 100-μm point source in Fig. 7a, b. The spatial resolution was estimated to be 220-μm FWHM (Fig. 7c). Assuming the spatial resolution distribution and source distribution are Gaussian, the spatial resolution of Cerenkov-light image corrected for the point source size (100 μm) is estimated to be ∼200 μm.

Figure 8 shows the Cerenkov-light image and its profile of the slit phantom. All 500-μm slits were resolved.

2. *Imaging of distributed character phantom* We show Cerenkov-light images of the NU phantom with different measurement times in Fig. 9. At 120 min, we obtained a high-resolution image of the phantom.

3. *Imaging of small animals* We show Cerenkov-light images of the tumor model rat in Fig. 10. We distinguished the accumulation of the ^{18}F-FDG in the tumor.

We show another study of the Cerenkov-light image of a model rat's tumor in Fig. 11. The accumulations of tumors were moderate. High accumulation of ^{18}F-FDG in the eyes and the brain were observed in the Cerenkov-light image.

We show Cerenkov-light images of a normal rat in Fig. 12. A high accumulation of ^{18}F-FDG in the eyes was observed. We show another study of Cerenkov-light images of a normal rat in Fig. 13a. We also observed the accumulation of ^{18}F-FDG in the eyes. We show a PET image of the rat in Fig. 13b. Accumulations of ^{18}F-FDG were observed on both sides of the Harderian gland and the brain. The fused image shows the difference of the high Cerenkov-light emission area and the FDG accumulation measured by PET.

We show the Cerenkov-light image of the rat's whole brain in Fig. 14. We observed some structures of the brain in the Cerenkov-light image.

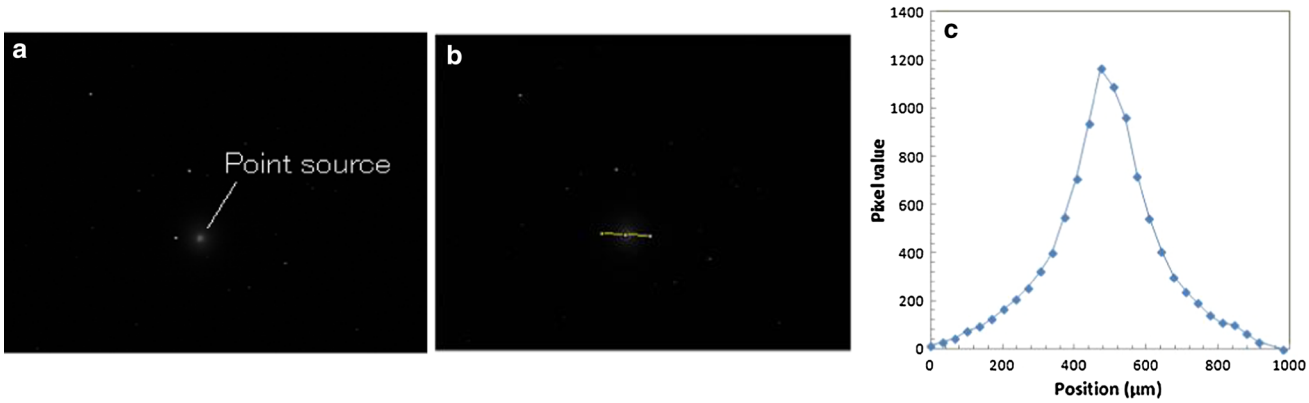

Fig. 7 Photo of 100-μm-diameter ^{22}Na point source (**a**), profile for the point source (**b**), and point spread function of the point source (**c**)

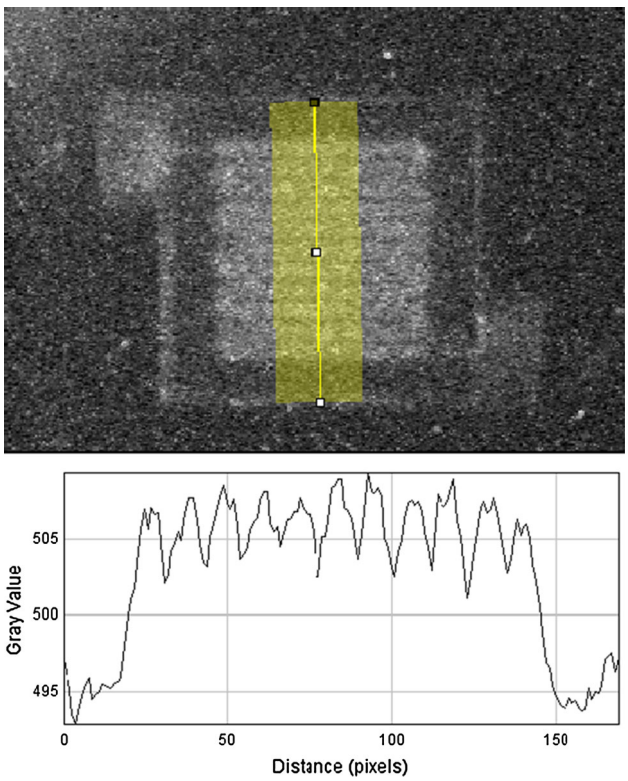

Fig. 8 Cerenkov-light image of the slit phantom (*upper*) and profile of the slits (*lower*)

We show an optical photo of a rat brain's slice in Fig. 15a and a Cerenkov-light image and a positron image with a CWO scintillator in Fig. 15b, c.

We show the vertical direction profiles of the Cerenkov-light and positron images with a CWO scintillator in Fig. 16a, b. Also, we show the horizontal direction profiles of the Cerenkov-light and positron images with a CWO scintillator in Fig. 16c, d. The edges were steeper in the Cerenkov-light image, but the image contrast was higher in the CWO scintillator images.

Discussion

We successfully developed a Cerenkov-light imaging system and conducted imaging for phantoms as well as ^{18}F-FDG administered in vivo and ex vivo rat studies. The spatial resolution of the Cerenkov-light imaging is 220 μm, which is much higher than that of the ultrahigh-resolution PET system [18] and probably higher than that of scintillator-based positron autoradiography. Such high resolution will be useful for distinguishing smaller parts of the subjects. In fact, the edges of the ex vivo rat brain showed sharper edges in the Cerenkov-light images than scintillator-based autoradiography (Fig. 16).

Another advantage of Cerenkov-light images is that a relatively simple and lower cost detector is needed for imaging the positron's distribution. A high-sensitivity CCD camera is easier to use and cheaper than PET systems.

However, the biggest disadvantage of Cerenkov-light imaging is that its distribution is different from the actual positron distribution. A typical example is the ^{18}F-FDG studies of rat heads, in which the Cerenkov light was detected in the rat's eyes, while the actual distribution was in the Harderian glands (Figs. 12, 13). This phenomenon can be explained: since the Harderian glands are located just behind the eyeballs, the Cerenkov light in the Harderian glands enters and passes through the eyeballs and is emitted from them. Such discrepancies might occur in other parts of the body in Cerenkov-light images.

Another disadvantage of Cerenkov-light images is that Cerenkov-light imaging can only image the distribution of positrons on the surface or areas surrounded by transparent materials. Consequently, the spatial resolution of the Cerenkov-light images and the signal to noise (S/N) are degraded due to the light's spread and absorption. We need to apply smoothing to Cerenkov-light images to reduce the statistical noise in the surface

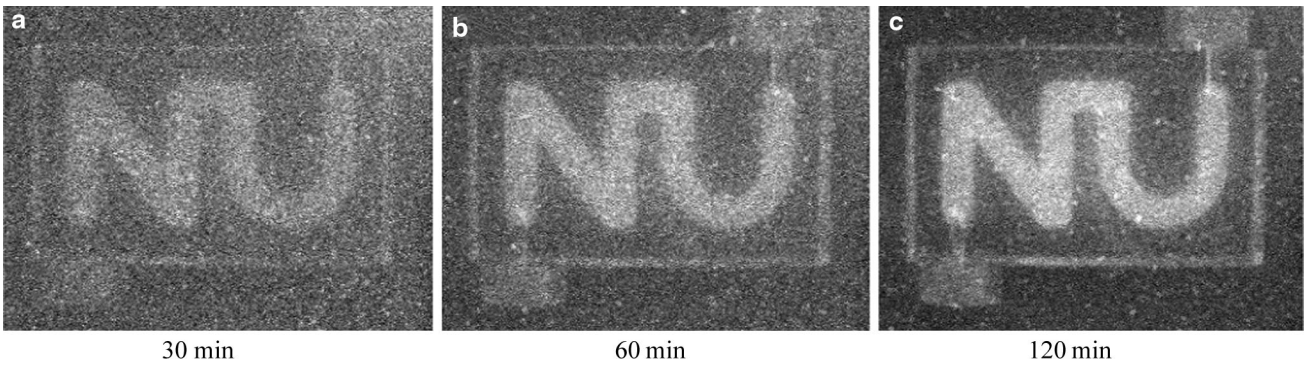

Fig. 9 Cerenkov-light image of the NU phantom with different measurement times

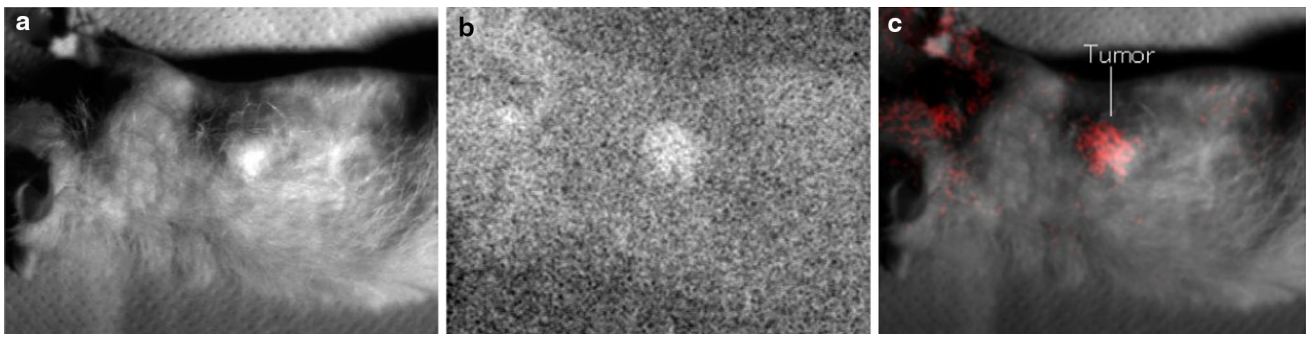

Fig. 10 Optical photo of model rat's tumor (**a**), Cerenkov-light image (**b**), and fused image (**c**): *color parts* are from Cerenkov-light image

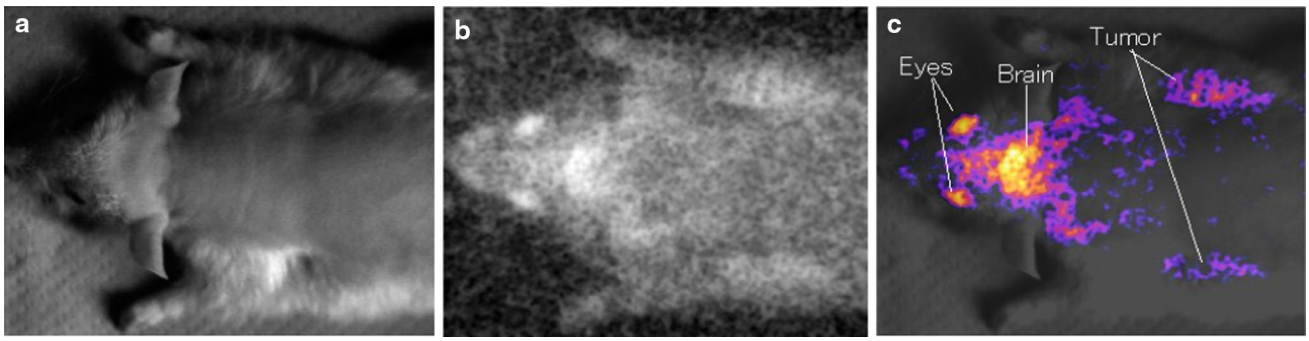

Fig. 11 Optical photo of a model rat's tumor (**a**), Cerenkov-light image (**b**), and fused image (**c**): *color parts* are from Cerenkov-light image

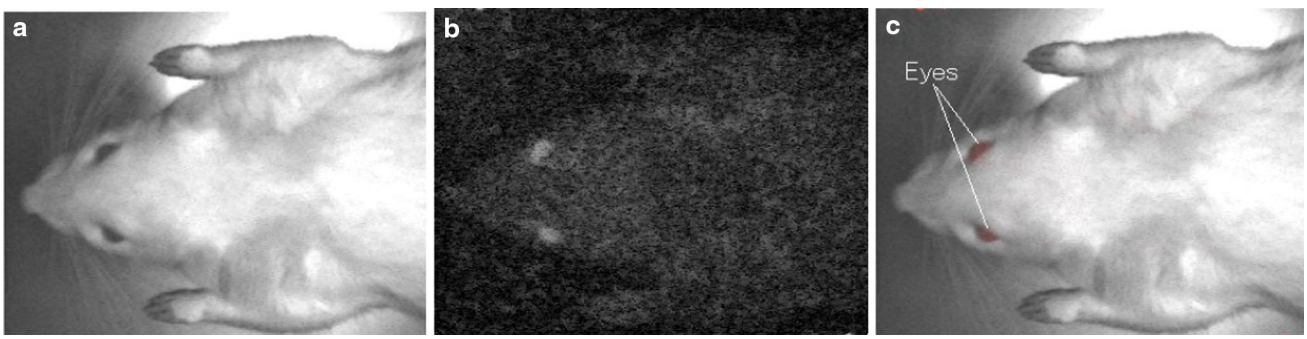

Fig. 12 Optical photo of a model rat's tumor (**a**), Cerenkov-light image (**b**), and fused image (**c**): *color parts* are from Cerenkov-light image

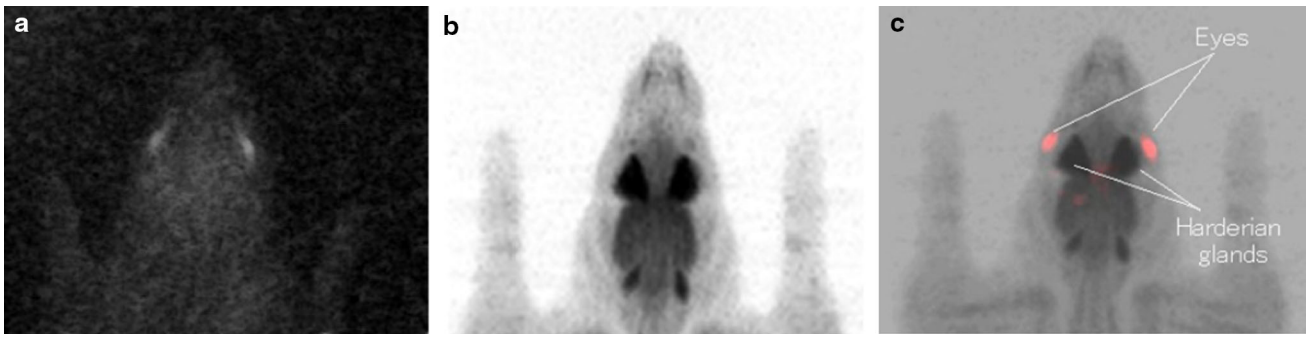

Fig. 13 Cerenkov-light image of rat (**a**), small animal PET image (**b**), and fused image (**c**): *color parts* are from Cerenkov-light image

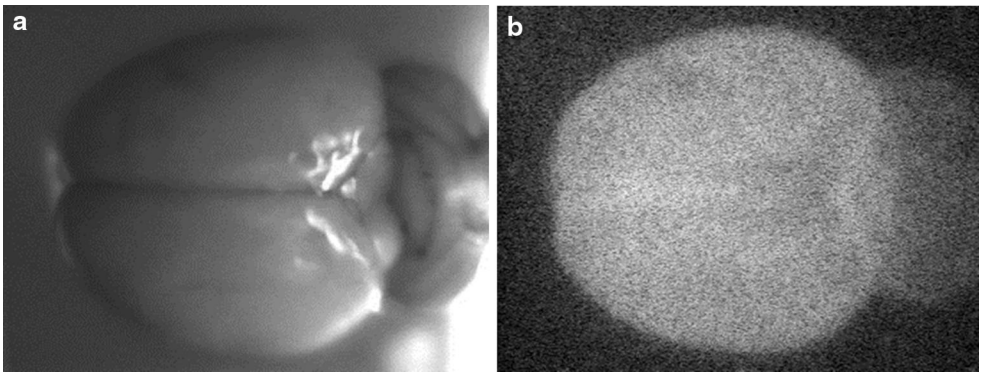

Fig. 14 Whole brain of a rat: optical photo (**a**) and Cerenkov-light image (**b**)

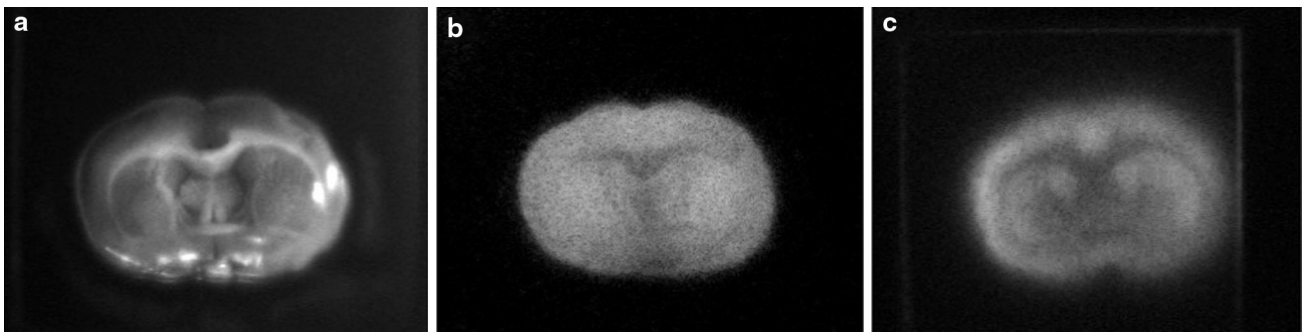

Fig. 15 Optical photo of a rat brain slice (**a**), Cerenkov-light image (**b**), and positron image with CWO scintillator (**c**)

images (Figs. 10, 11), which also degrades their spatial resolution. Another disadvantage is the low contrast that we mainly observed in the ex vivo studies, where the sliced images had significant background intensity (Figs. 14, 15). This is probably because the Cerenkov light, which was produced in the deeper position of the slice detected on the surface of the slice, decreased the contrast of the images. A very strict light shield for the measurements is another disadvantage of Cerenkov-light imaging. Cerenkov light is so weak that subjects must be set inside a black box.

Conclusion

We could successfully develop a Cerenkov-light imaging system and image various types of subjects with the system to explore the usefulness of the system. We found that although Cerenkov-light images showed ultrahigh resolution of $\sim$220 μm for phantom studies, their distribution and contrast were sometimes different from the actual positron accumulation in rat in vivo and ex vivo studies. Even though the spatial resolution on the surface is high, care must be taken when evaluating

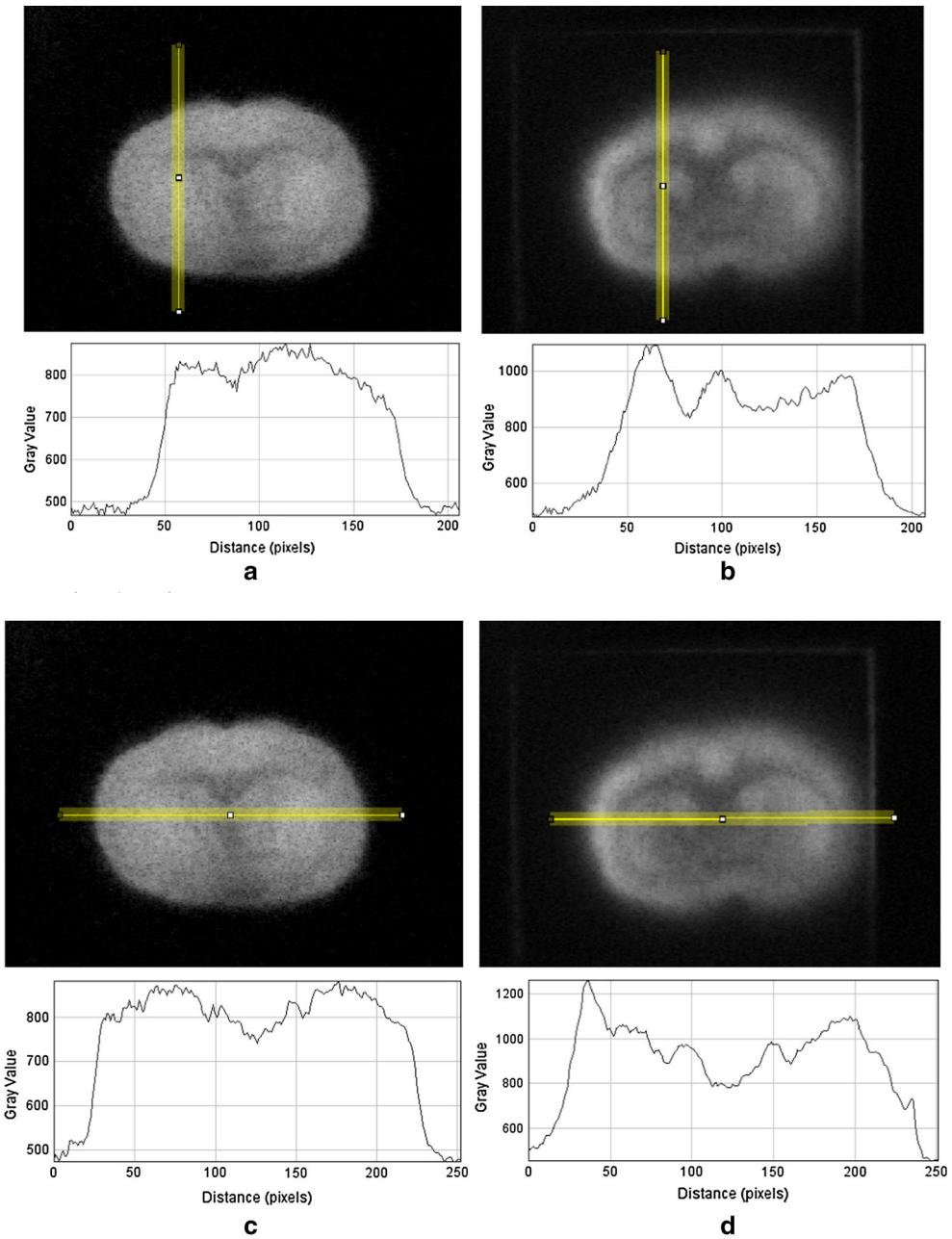

Fig. 16 *Vertical direction* profiles of Cerenkov-light image (**a**), positron image with CWO scintillator (**b**), *horizontal direction* profiles of Cerenkov-light image (**c**), and positron image with CWO scintillator (**d**)

the position distribution for Cerenkov-light images. However, the ultrahigh resolution of Cerenkov-light imaging will be useful at least for transparent subjects including phantom studies.

Acknowledgments This work was partly supported by the Japan Science and Technology Association and Ministry of Education, Science, Sports and Culture, Japan.

References

1. Robertson R, Germanos MS, Li C, Mitchell GS, Cherry SR, Silva MD. Optical imaging of Cerenkov light generation from positron-emitting radiotracers. Phys Med Biol. 2009;54:N355–65.
2. Spinelli AE, D'Ambrosio D, Calderan L, Marengo M, Sbarbati A, Boschi F. Cerenkov radiation allows in vivo optical imaging of positron emitting radiotracers. Phys Med Biol. 2010;55:483–95.
3. Knoll G. Radiation detection and measurement. 3rd ed.

4. Cho JS, Taschereau R, Olma S, Liu K, Chen YC, Shen CK, et al. Cerenkov radiation imaging as a method for quantitative measurements of beta particles in a microfluidic chip. Phys Med Biol. 2009;54:6757–71.
5. Liu H, Ren G, Miao Z, Zhang X, Tang X, Han P, et al. Molecular optical imaging with radioactive probes. PLoS ONE. 2010;5:e9470.
6. Liu H, Ren G, Liu S, Zhang X, Chen L, Han P, et al. Optical imaging of reporter gene expression using a positron-emission-tomography probe. J Biomed Opt. 2010;15:060505.
7. Ruggiero A, Holland JP, Lewis JS, Grimm J. Cerenkov luminescence imaging of medical isotopes. J Nucl Med. 2010;51:1123–30.
8. Park JC, Il An G, Park SI, Oh J, Kim HJ, Su Ha Y, et al. Luminescence imaging using radionuclides: a potential application in molecular imaging. Nucl Med Biol. 2011;38(3):321–9.
9. Hu Z, Liang J, Yang W, Fan W, Li C, Ma X, et al. Experimental Cerenkov luminescence tomography of the mouse model with SPECT imaging validation. Opt Expr. 2010;18:24441–50.
10. Park JC, Yu MK, An GI, Park SI, Oh J, Kim HJ, et al. Facile preparation of a hybrid nanoprobe for triple-modality optical/PET/MR imaging. Small. 2010;6:2863–8.
11. Boschi F, Calderan L, D'Ambrosio D, Marengo M, Fenzi A, Calandrino R, et al. In vivo 18F-FDG tumour uptake measurements in small animals using Cerenkov radiation. Eur J Nucl Med Mol Imaging. 2011;38:120–7.
12. Xu Y, Liu H, Cheng Z. Harnessing the power of radionuclides for optical imaging: Cerenkov luminescence imaging. J Nucl Med. 2011;52(12):2009–18.
13. Elrick RH, Parker RP. The use of Cerenkov radiation in the measurement of betaemitting radionuclides. Int J Appl Radiat Isot. 1968;19:263–71.
14. Jelley JV. Cerenkov radiation and its applications. Br J Appl Phys. 1955;6:227–32.
15. Rasband, WS, ImageJ, US National Institutes of Health, Bethesda, MD, USA. 1997–2012. http://imagej.nih.gov/ij/.
16. Schneider CA, Rasband WS, Eliceiri KW. NIH Image to ImageJ: 25 years of image analysis. Nat Methods. 2012;9:671–5.
17. Constantinescu CC, Mukherjee J. Performance evaluation of an Inveon PET preclinical scanner. Phys Med Biol. 2009;54(9):2885–99.
18. Yamamoto S, Watabe H, Kanai Y, Watabe T, Kato K, Hatazawa J. Development of an ultrahigh resolution Si-PM based PET system for small animals. Phys Med Biol. 2013;58(21):7875–88.